Iranian Journal of Geophysics, 2020, Page 60 - 78

RESIP2DMODE: A MATLAB-Based 2D Resistivity and Induced Polarization Forward Modeling Software

Reza Ghanati [1*], Yosra Azadi [2] *and* Razieh Fakhimi [2]

[1] *Assistant Professor, Institute of Geophysics, University of Tehran, Tehran, Iran*
[2] *M.Sc. Student, Institute of Geophysics, University of Tehran, Tehran, Iran*

(Received: 01 December 2019, Accepted: 22 January 2020)

Abstract

Forward modeling is an integral part of every geophysical modeling resulting in the numerical simulation of responses for a given physical property model. This Forward procedure is helpful in geophysics both as a means to interpret data in a research setting and as a means to enhance physical understanding in an educational setting. Calculation of resistivity and induced polarization forward responses is carried out using simulation of the current flow into the earth's surface through solving the Poisson's equation. In this contribution, a finite-difference algorithm is applied to discretize the simulated models restricted by a mixed boundary condition. To account for the 3D source characteristic, a spatial Fourier transform of the partial differential equations with respect to a range of wave numbers is performed along the strike direction. Then, an inverse Fourier transformation is conducted to obtain the potential solutions in the spatial domain. The present package provides a user-friendly interface designed to understand and handle for various conventional electrical configurations in the frame of the MATLAB programming language. To verify the program, initial responses of some simple models are compared with those of analytic solutions, which proved satisfactory in terms of accuracy. For further evaluation, the code is also examined on some complicated models.

Keywords: RESIP2DMODE, Resistivity, Chargeability, Forward modeling, MATLAB, Finite-difference

*Corresponding author: rghanati@ut.ac.ir

1 Introduction

Electrical resistivity tomography (ERT) is commonly used to provide an image of the variation of the subsurface electrical properties based on some surface or borehole measurements. Typical applications arise in the hydrogeological, environmental, and archaeological problems. On the other hand, it has been shown that time-domain induced polarization can significantly enhance the information for environmental and engineering applications (e.g., Dahlin et al., 2010; Gazoty et al., 2012). An accurate model of the earth's subsurface is highly depended upon the forward calculation, which is implemented inside of the inverse algorithm. Several attempts have been made in the numerical solution of the forward problem for a two dimensional resistivity distribution. For instance, Dey and Morrison (1979a) presented the basis for the forward computation based on finite-differences. An improvement of boundary conditions was given by Zhang et al (1995). Lowry et al. (1989) improved the quality of the modeling results by the singularity removal technique. They split up the total potential into a known reference potential of a background model and a secondary potential due to conductivity deviations from the background model, which results in accurate numerical calculations of the second potential on moderate grids. Spitzer and Wurmstich (1995) dealt with speed and accuracy of different discretization schemes and equation solvers. Due to the rapid advancement of computers, it is now possible to carry out accurate numerical solutions for large models with high resistivity contrasts (Günther, 2004; Günther et al., 2006). The direct-current geo-electrical forward problem is also solved by the finite element methods, for instance: Hughes (1987), Wu (2003); Rücker et al. (2006), Demkowicz (2007); and Qiang et al. (2013). Likewise, Mendez-Delgado et al. (1999) applied a semi-analytical algorithm based on integral equations for forward modeling of the direct current and low-frequency electromagnetic fields. Recently, Yuan et al. (2016) took advantage of the finite-element–infinite-element coupling method for 2.5D resistivity forward modeling with computationally more efficient functionality. Additionally, some 2D and 3D resistivity modelling packages have been provided with special emphasis on the inversion process. For instance, pyGIMLi developed by Rücker et al. (2017) is a Python library for 2D inversion of electrical resistivity data. ELRIS2D (Akca, 2016) is a Matlab-based package for 2D inversion of DC resistivity and IP data. Befus (2018) proposed PYRES a Python wrapper for electrical resistivity modeling with R2. Pidlisecky and Knight (2008) presented a 2.5-D inverse modeling algorithm for electrical resistivity data. Despite the significant developments in numerical procedures of calculation of resistivity and induced polarization forward responses, it is still an extensively open-research area. In this paper, a two-dimensional resistivity and induced polarization forward modeling program named RESIP2DMODE is presented. The main advantages of the package is its user-friendly interface property and it provides students and researchers with a simple code aiming at more knowledge about the process of a 2D electrical resistivity and induced polarization modeling so that one can simply modify or improve any part of the program based on his/her demands. The program was written and evaluated on the MATLAB versions R2016a and R2018b resulting in full functionality. The paper continues with a review of the resistivity and induced polarization forward algorithm in section 2. In section 3, a short description of the algorithm implementation and example simulations is presented. The program is evaluated

based on the performance comparison results of analytic solutions and those of the package on horizontal and vertical layers along with further investigation using some complex synthetic examples in section 4. Section 5 provides a discussion on the solutions derived from the proposed package compared to the analytical results. The conclusions are drawn in section 6.

2 Methodology

In this section, we briefly review the mathematical formulation required to construct the forward modeling program. The modeling of the electrical potential is stated in terms of the partial differential equations. The numerical solution of the differential equations requires that they are transformed into algebraic form. This is carried out by the method of finite-differences, by which the continuous variables are represented by their values at a finite set of points, and derivatives are approximated by differences between values at adjacent points.

Governing equations

The current density $\boldsymbol{J}$ is related to the electric field $\boldsymbol{E}$ by the conductivity ρ of the medium denoted by Ohm's law

$$\boldsymbol{J} = \frac{1}{\rho}\boldsymbol{E} \tag{1}$$

Since the electric field is stationary, it can be written as:

$$\begin{aligned} &\boldsymbol{\nabla} \times \boldsymbol{E} = 0 \\ &\boldsymbol{E} = -\boldsymbol{\nabla}\mathrm{P} \end{aligned} \tag{2}$$

where P is scalar potential.

The partial differential equations governing the resistivity problem is obtained by using the principle of conservation of charge and the continuity equation, we have for a point source $r_s(x_s.\, y_s.\, z_s)$

$$\boldsymbol{\nabla} \cdot \boldsymbol{J} = I\delta(x - x_s)\delta(y - y_s)\delta(z - z_s) \tag{3}$$

I is the current injected into the subsurface earth at r_s. With combining all of the above relations, we get:

$$\begin{aligned} &-\boldsymbol{\nabla} \cdot [\sigma(x.\, y.\, z)\boldsymbol{\nabla}\mathrm{P}(x.\, y.\, z)] \\ &= I\delta(x - x_s)\delta(y - y_s)\delta(z - z_s) \end{aligned} \tag{4}$$

In addition, considering Ohm's law for a two-dimensional conductivity model, as:

$$\boldsymbol{J} = -\sigma(x.\, z)\boldsymbol{\nabla}\mathrm{P} \tag{5}$$

with combining (3) and (5):

$$\begin{aligned} &\boldsymbol{\nabla}^2\{\sigma(x.\, z)\mathrm{P}(x.\, y.\, z)\} \\ &\qquad + \sigma(x.\, z)\boldsymbol{\nabla}^2\mathrm{P}(x.\, y.\, z) \\ &-\mathrm{P}(x.\, y.\, z)\boldsymbol{\nabla}^2\sigma(x.\, z) = \\ &-2I\delta(x - x_s)\delta(y - y_s)\delta(z - z_s) \end{aligned} \tag{6}$$

To account for the 3D source characteristic, a spatial Fourier transform of the partial differential equations with respect to different a range of wave numbers is performed along the strike direction (y).

$$\begin{aligned} &\widetilde{\mathrm{P}}(x.\, K_y.\, z) \\ &= \int_0^\infty \mathrm{P}(x.\, y.\, z)\cos(K_y y)\, dy, \end{aligned} \tag{7}$$

where $\widetilde{\mathrm{P}}$ indicates the transformed potential and K_y is the wavenumber with respect to y.

Applying the Fourier-cosine transformation to the 3D Poisson Equation (6) yields a 2D Helmholtz equation, given by:

$$\begin{aligned} &-\frac{\partial}{\partial x}\sigma(x.\, z) + \frac{\partial \widetilde{\mathrm{P}}}{\partial x} + K_y^2\sigma(x.\, z)\widetilde{\mathrm{P}} \\ &-\frac{\partial}{\partial z}\sigma(x.\, z)\frac{\partial \widetilde{\mathrm{P}}}{\partial z} = \frac{I}{2}\delta(x - x_s)\delta(z - z_s), \end{aligned} \tag{8}$$

The above equation is solved for a two-dimensional domain restricted by mixed boundary conditions. To numerically solve Equation (8), it is required to construct a discrete model in the form of a rectangular grid with nodes at the cell center. Then, the existing partial derivatives are replaced by finite-difference formulas. Hence, the two-dimensional modeling medium is subdivided into a grid by the node positions $X_i(i \in 1, 2, \dots, N)$ and $X_i(j \in 1, 2, \dots, M)$. Figure 1 shows the two-dimensional finite-difference grid used to discretize the transformed Equation (8). In addition, Figure 1 depicts a detailed description of the dashed area corresponding to the ij^{th} cell with the conductivity $\sigma_{i,j}$ bounded by the grid nodes $(i, j-1)$, $(i+1, j)$, $(i+1, j)$, and $(i-1, j)$.

By integration of Equation (8) over the corresponding cell, we get:

$$-\oint_{\partial D_{i.j}} \sigma(x.z)\frac{\partial \widetilde{\mathrm{P}}}{\partial \hat{n}}dl + K_y^2\int_{D_{i.j}} \sigma(x.z)\widetilde{\mathrm{P}}dA = \frac{I}{2}\int_{D_{i.j}} \delta(x-x_s)\delta(z-z_s)dA, \quad (9)$$

By expanding the left side of (9) and combining with other terms, it yields the coupling coefficients:

$$A_1\widetilde{\mathrm{P}}_{i-1.j} + A_2\widetilde{\mathrm{P}}_{i.j-1} + A_3\widetilde{\mathrm{P}}_{i.j} + A_4\widetilde{\mathrm{P}}_{i.j+1} + A_5\widetilde{\mathrm{P}}_{i+1.j} = \frac{I}{2}\delta(x-x_s)\delta(z-z_s), \quad (10)$$

where

$$A_1 = -\frac{\sigma_{i-1.j-1}\Delta z_{j-1} + \sigma_{i-1.j}\Delta z_j}{2\Delta x_{i-1}}$$

$$A_2 = -\frac{\sigma_{i-1.j-1}\Delta x_{i-1} + \sigma_{i.j-1}\Delta x_i}{2\Delta z_{j-1}} \quad (11)$$

$$A_3 = -\frac{\sigma_{i-1.j}\Delta x_{i-1} + \sigma_{i.j}\Delta x_i}{2\Delta z_j}$$

$$A_4 = -\frac{\sigma_{i.j-1}\Delta z_{j-1} + \sigma_{i.j}\Delta z_j}{2\Delta x_i}$$

$$A = -\left(C_L^{ij} + C_R^{ij} + C_T^{ij} + C_B^{ij}\right) + \frac{K_y^2}{4}\cdot \left(\sigma_{i.j}\Delta x_i\Delta z_j + \sigma_{i-1.j}\Delta x_{i-1}\Delta z_j\right) + \sigma_{i.j-1}\Delta x_i\Delta z_{j-1} + \sigma_{i-1.j-1}\Delta x_{i-1}\Delta z_{j-1},$$

where A_1, A_2, A_3, and A_4 are the coefficients in $-X$, $+X$, $+Y$, and $-Y$ (i.e., left, right, top, and bottom), respectively as well as A indicates the self-coupling coefficient. Having obtained discrete representations for the governing equations and boundary condition at all nodes, the transformed forward problem can be written as a system of equations

$$\boldsymbol{A}\widetilde{\mathrm{P}} = \boldsymbol{S} \quad (12)$$

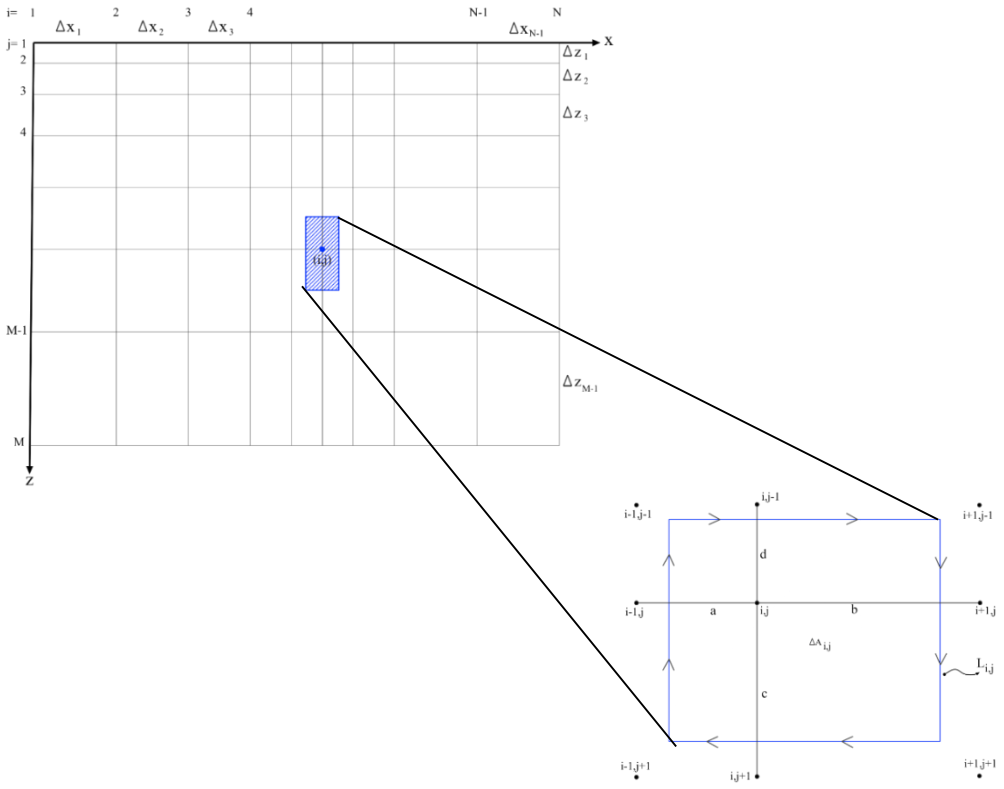

Figure 1: Two-dimensional finite-difference grid and a detained description of the dashed area corresponding to the ij^{th} cell with the conductivity $\sigma_{i,j}$.

A is the Capacitance Matrix and is a function of the geometry and the physical property distribution, and vector $\boldsymbol{S}$ is related to source location represented as a discrete delta Dirac function. The recent equation has to be solved for the vector $\widetilde{\mathrm{P}}$ containing the potentials for all existing nodes. After computing the Fourier transformed solutions for a sufficiently large number of discrete wavenumbers, an inverse Fourier transform is implemented to obtain the potential solutions in the spatial domain. Note that further details about the solution of the governing equations as well as the discretization of the model in terms of the finite difference algorithm can be found in Dey and Morrison (1997a) and McGillivray (1992).

Induced polarization forward modeling is introduced to describe the polarization property of the Earth's subsurface, namely chargeability. The response of a 2D chargeability model in the time domain can be computed using Equation in which the direct current geo-electrical resistivity forward operator is calculated with respect to the conductivity models (σ) and ($\sigma - \mathcal{M}$).

$$\mathcal{M}_a = \frac{\mathcal{R}(\sigma - \mathcal{M}) - \mathcal{R}(\sigma)}{\mathcal{R}(\sigma - \mathcal{M})} \qquad (13)$$

where $\mathcal{R}$ is the resistivity forward operator, $\mathcal{M}_a$ is the apparent chargeability, σ and $\mathcal{M}$ indicate the true conductivity chargeability models, respectively. From the above equation, it is evident that the apparent chargeability is calculated based on the twice implementation of the resistivity forward operator for two conductivity models (σ) and ($\sigma - \mathcal{M}$).

3. Program Implementation

The aim of the software is to present a flexible solution for resistivity and induced polarization forward calculation that works based on the finite-difference algorithm due to the fast computational time. Base on the principle of numerical simulation, the precision of the results increases with increasing numerical effort in the form of a finer discretization. Hence, it is required to pay attention to find a trade-off between reasonable accuracy within limited computing time. The package consists of three main scripts:

- PotentialInitial.m is applied to calculate the electrical potential distribution for the first electrode position in terms of different wave numbers. Whereas in the forward modeling, the capacitance matrix is a function of the geometry of the survey and the physical property distribution, for multiple current electrode positions this matrix remains unaltered, and consequently, only one inverse of the matrix in terms of different wave numbers provides the solution to different sets of potential distribution for the different source positions. This strategy reduces the computational process. Hence, after pressing the Run button (Figure 7), it takes time to produce the inverse of the capacitance matrices with respect to the wave numbers for the first electrode location. However, this time relies on the parameters defined in the survey parameters box.
- PotentialCal.m is implemented to calculate the electrical potential for the rest of the electrode positions (except the first electrode position) using the inverted capacitance matrices from PotentialInitial.m.
- INVCal.m is utilized to invert the capacitance matrices created in PotentialInitial.m.
- RESIP2DMODE.m is the main source code which includes the user interface functions, the apparent resistivity calculation codes, and the plotting functions.

Figure 2 shows the basic architecture of RESIP2DMODE written in the MATLAB programming language. A graphical user

interface of the program is generated for ease of use and simplicity. Any change in the options is imposed immediately on the input parameters. A view of the user interface is depicted in Figure 3. The implementation of the program begins with inserting some information about the configuration, geometry of survey (e.g., number of stations, electrode spacing, and number of pseudo-section levels). There is no limitation in the choice of the survey parameters, but it should be noted that increasing the computational medium would cause a higher computation time and storage space. Figure 4 shows survey parameters setting menus where the type of array including the most common configuration, number of stations, number of pseudo-section data levels (this parameter depends upon the type of array), amount of the injection current and number of nodes per electrode spacing in discretization of the work area. The latter parameter can be selected arbitrarily but with respect to computational time and accuracy in numerical modeling. You can choose a mesh grid having 2 or 4 nodes between adjacent electrodes. With 4 nodes per electrode spacing, the calculated apparent resistivity values would be more accurate, in particular, for large resistivity contrasts.

Once the survey characteristics have been chosen, the user should set the discretization parameters in the Z direction based on a logarithmic function that will be used to generate the vertical direction of the computational area. According to Figure 5, the minimum depth is set 0 because the discretization begins from the earth's surface, the maximum depth of discretization is chosen with respect to the dimension of the modeling area and considering the boundary conditions. Likewise, the user can set the number of layers. Note that the discretization should be very dense in the shallow part of the model and coarse in the deeper part of the model. Once these parameters have been set, the user needs to press the set-layering button to implement the changes required and then the creation of an output file named Layering.xls, which consists of the depth of each layer from the surface. The next step is to insert the model parameters in terms of conductivity (S/m) and chargeability (msec) (Figure 6). The number of values depends on the variety of anomalies in the simulated model.

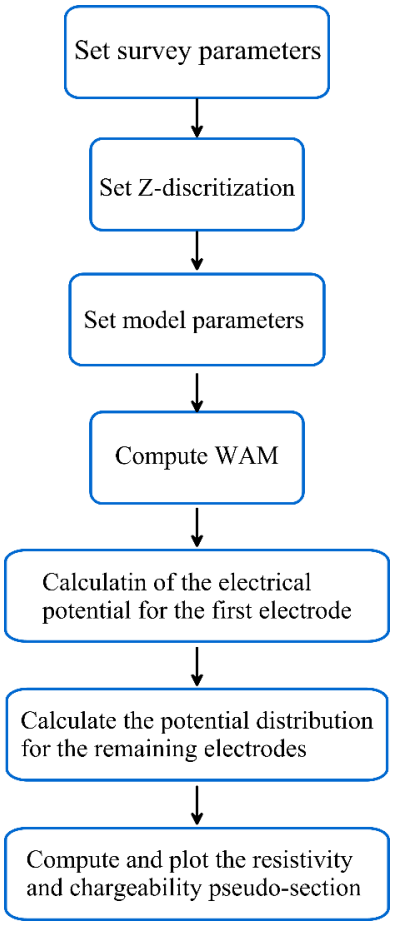

Figure 2. Flowchart of the forward modelling program.

After determining the required parameters of the modeling, it is time to generate the discretized work area by pressing the create WAM button, which results in an output file named WAM.xlsx (Figure 7). The WAM file provides a section to the user to construct any arbitrarily model by assigning integer values $(0, 1, 2, ...)$ to the physical parameters defined in the model

parameters box (Figure 3). An example of the WAM.xlsx filled with the integer values associated to Example 1 is illustrated in Figure 8. Note that you only have to set the resistivity values for a limited section of finite difference grid model. The program assumes that the resistivity of the blocks to the left side of the first electrode is the same as that of the first model block for which you have set the resistivity value. Similarly, the resistivity of the blocks on the right side are set to be the same as that of the last block of the rightmost column in the user-defined model section.

4. Numerical Experiments

4.1 Numerical versus analytical solutions

In order to evaluate the accuracy and effectiveness of our numerical modeling routine, we present two examples that compare the numerical results with those from the analytical solutions (see Telford et al., 1991). We first simulate a two-layer medium with the geo-electrical parameters indicated in Figure 9. Electrical sounding using Pole-Dipole, and Dipole-Dipole configurations above the model are conducted. The results of the apparent resistivity distributions derived from numerical and analytical

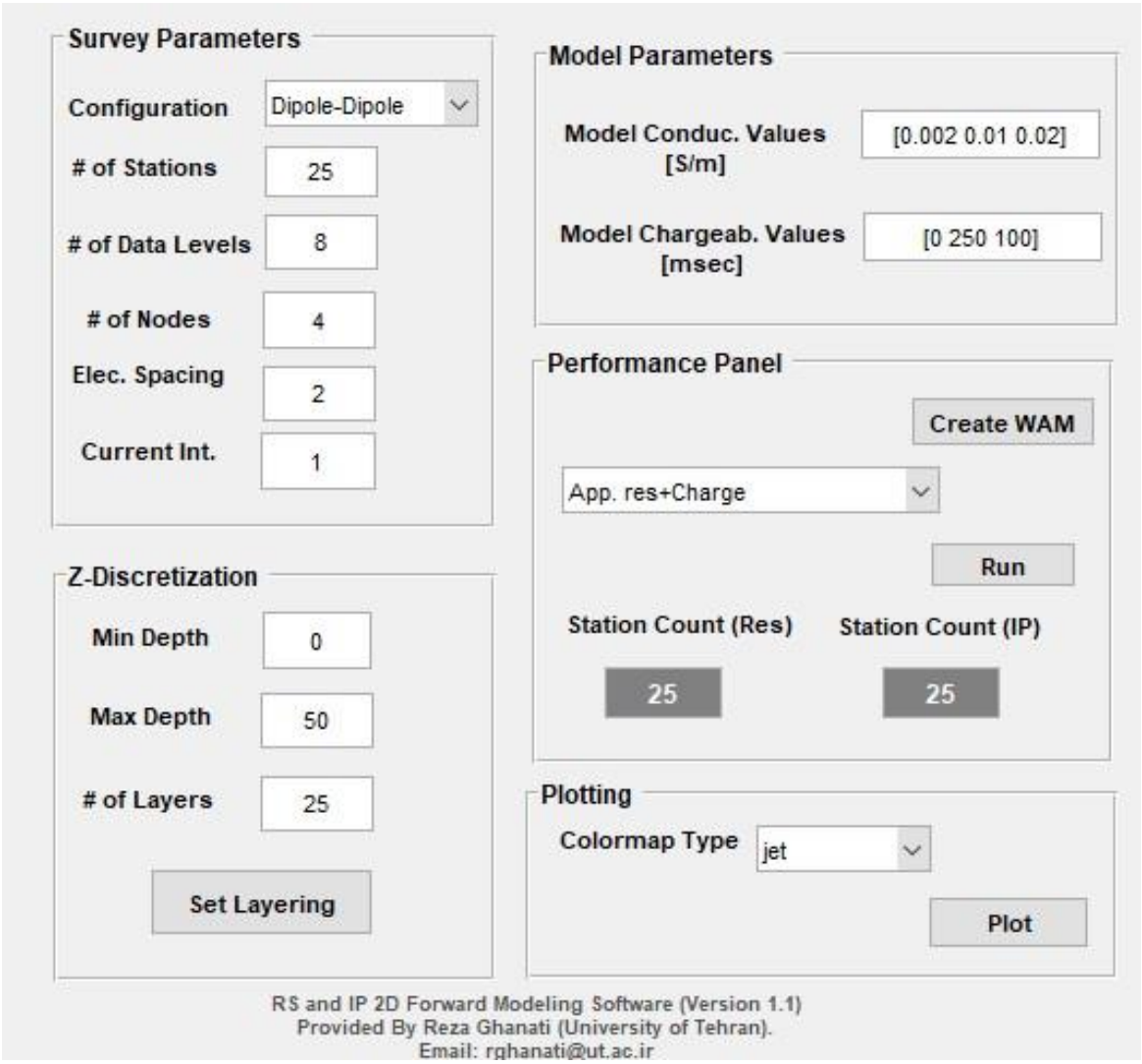

Figure 3. A view of the user interface of the program.

schemes are given in Table 1. Furthermore, the relative errors (i.e., $\frac{\|\rho^* - \rho\|_2}{\|\rho^*\|_2}$, where ρ^* is the exact solution and ρ is the numerical solution obtained from the analytical solutions and the proposed software, respectively) between the analytical and numerical results are represented in Table 1. Referring to Table 1, it can be observed that the relative errors of all simulations associated to Pole-Dipole and Dipole-Dipole are 5.66% and 7.1%, respectively, which shows an appropriate accuracy of the forward package. The second model is a vertical contact as shown in Figure 10 for comparing the electrical resistivity distribution errors among an analytical solution and the numerical solution obtained from Pole-Pole measurements. The simulation is computed with the same discrete domain size. The results are reported in Table 2 where the relative error between the analytical solution and numerical solution is 6.48%.

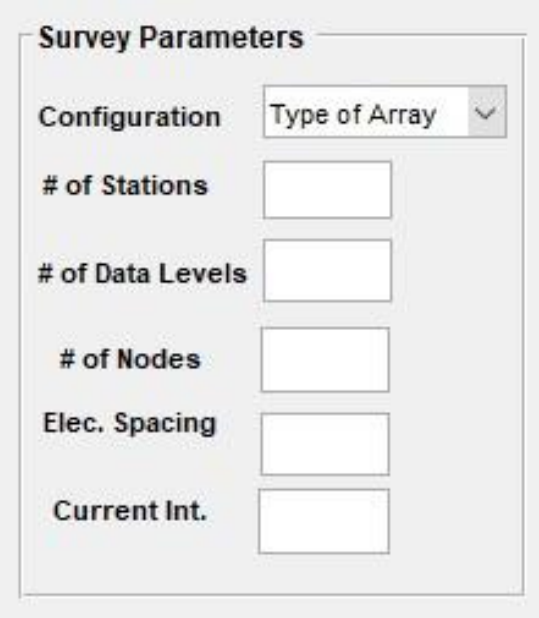

Figure 4. Image of the survey parameters setting menu.

Table 1: Comparison between the apparent resistivity values obtained from the analytical solutions and numerical results along with the relative errors associated to the two-layer earth model through Dipole-Dipole and Pole-Dipole configurations.

Analytic solution	Dipole-Dipole	101.83	98.09	85.8	69.25	53.25	40.20	30.55	23.84	19.33	16.37	Relative error (%) DD	Relative error (%) PD
	Pole-Dipole	94.44	79.65	61.22	44.83	32.61	24.36	19.08	15.8	13.79	12.56		
Numerical solution	Dipole-Dipole	107.41	101.08	89.62	74.27	58.86	45.7	35.46	27.88	22.4	18.44	5.66	7.1
	Pole-Dipole	97.41	80.79	63.26	47.71	35.84	27.58	22.15	18.71	16.58	15.28		

Table 2: Comparison between the apparent resistivity values obtained from the analytical solutions and numerical results along with the relative errors associated to the vertical contact earth model through the Pole-Pole configuration.

Analytic solution	**Pole-pole**	10.33	10.35	10.38	10.41	10.45	10.50	10.56	10.64	10.73	10.8	11.06	11.37	11.92	13.20	19.6	19.6	339.8	403.9	431.37	446.62	Relative error (%) PP
Numerical solution	**Pole-Pole**	12.28	12.49	12.56	12.61	12.66	12.72	12.79	12.87	12.98	13.10	13.36	13.66	14.22	15.5	22.48	22.45	363.4	431.9	460.7	476.8	6.48

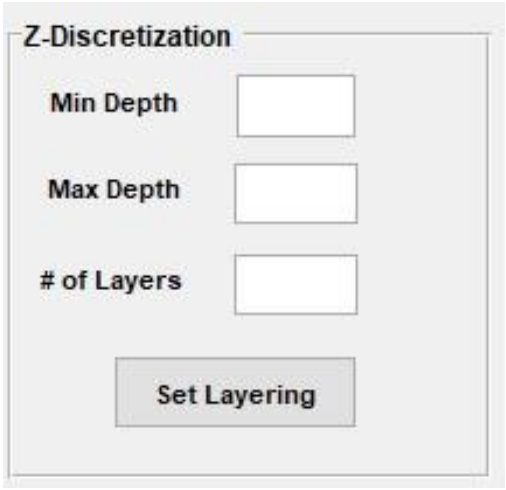

Figure 5. Image of the Z-discretization setting menu.

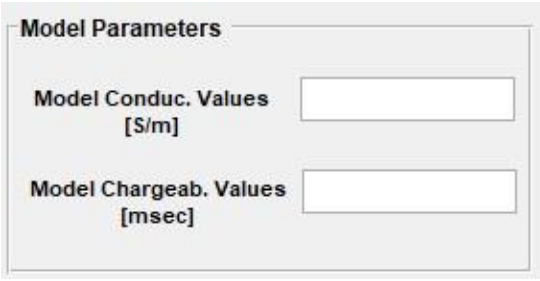

Figure 6. Image of the model parameters setting menu.

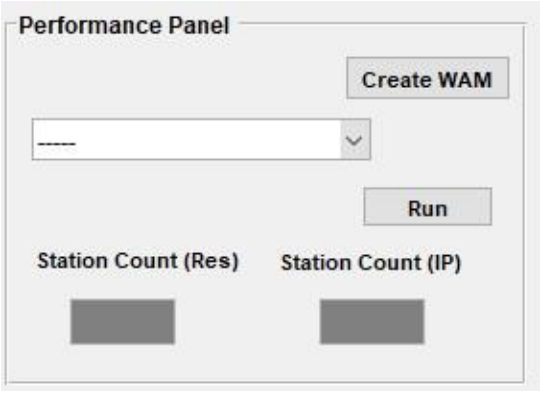

Figure 7. Image of the performance parameters setting menu.

4.2 Complex models

To further verify the efficiency of the software, two synthetic examples including a simple model generated from two embedded blocks and a complicated model constructed from an inclined contact and a block are simulated. The first example contains two blocks buried in $500\ \Omega \cdot m$ half-space at 2.11 m from the ground surface. The left block is $6\ m \times 1.87\ m$ with the resistivity of $100\ \Omega \cdot m$, and the right block is $6\ m \times 1.87\ m$ with $50\ \Omega \cdot m$ resistivity. To calculate the induced polarization pseudo-section, the chargeability values of the background, left and right bodies are set as 0, 250, and 100 msec, respectively. Figures 11(b) and (d) show the true resistivity and chargeability models associated with Example 1, respectively. For both examples, the apparent resistivity and chargeability responses of the simulated models are computed using collinear Dipole-Dipole and Wenner arrays assuming a multi-electrode system with 25 take-outs is used. The survey and discretization parameters assumed to calculate the DC resistivity and time-domain chargeability corresponding to the synthetic models 1 and 2 are represented in Table 3. Figures 11 and 13 show the apparent resistivity and chargeability contours for the simple model and for the Wenner and Dipole-Dipole configurations, respectively. It is seen from the pseudo-sections that there are obviously two low-resistivity anomalies and two high-chargeability anomalies, approximately in agreement with the assumed anomalies. Furthermore, for better evaluation of the results, a comparison of the values of the apparent resistivity and chargeability computed by a commercial software named RES2DMOD ver. 3.01 (Loke, 2014) are represented in Figures 12 and 14, respectively. Visually comparing the resulting pseudo-sections, it is evident that there is a trivial difference between the apparent resistivity and chargeability contours obtained from the presented software and RES2DMOD.

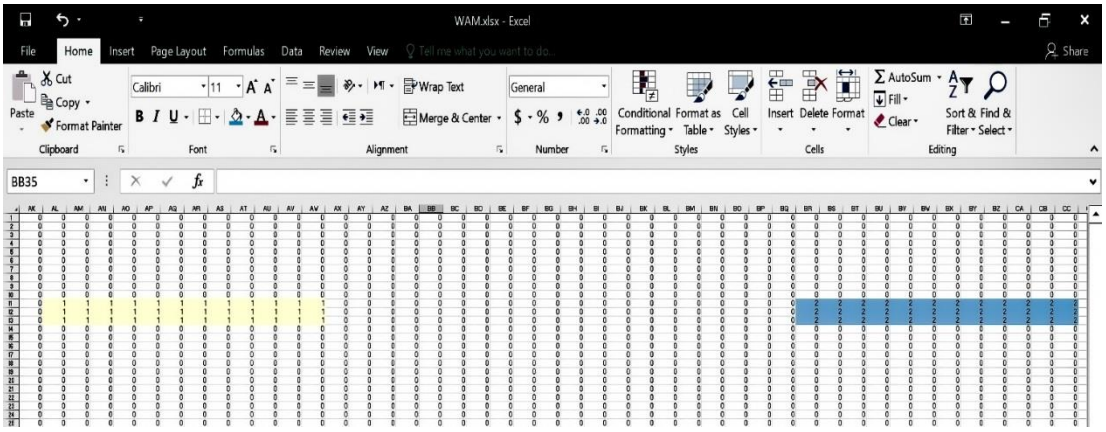

Figure 8. Image of the model generated in Excel Spreadsheet corresponding to Example 1.

Table 3: Assumed survey and discretization parameters for synthetic models 1 and 2.

Survey and discretization parameters	Model 1	Model 2
Number of Stations	25	25
Number of Data Levels	8	10
Number of nodes	4	4
Electrode spacing	2	3
Current intensity (A)	1	1
Minimum depth (m)	0	0
Maximum depth (m)	50	50
Number of Layers	25	25

In the second example (see Figure 15 (b)), the earth model contains a $200\ \Omega \cdot m$ inclined contact in $100\ \Omega \cdot m$ background as well as a block with resistivity of $400\ \Omega \cdot m$. In the case of the chargeability values (see Figure 15 (d)), the background, inclined contact, and embedded block are 50, 200, and 100 msec, respectively. Note that there is no topography included into the synthetic earth models. The resistivity and chargeability pseudo-sections associated to Examples 2 are illustrated in Figures 15(b) and (d) for the Wenner array and Figure 17(b) and (d) for the Dipole-Dipole array, respectively. From the pseudo-sections, it is obvious that the anomalies with high resistivity and chargeability values are detectable using both configurations. Moreover, it can be observed that the Dipole-Dipole array gives a wider horizontal coverage and smaller depth of investigation compared to the Wenner pseudo-section. The geo-electrical pseudo-sections are also

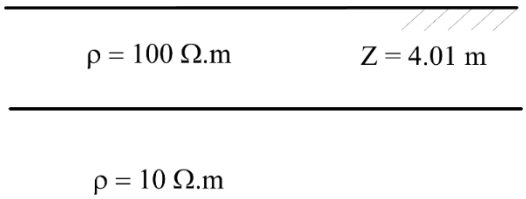

Figure 9. A two-layer model. The resistivity values of the first layer and the second layer are $100\ \Omega.m$ and $10\ \Omega.m$, respectively, with a thickness of 4.01 m.

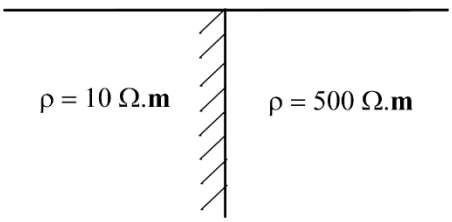

Figure 10. A vertical contact model used to illustrate the accuracy of our modelling algorithm with resistivity values of $10\ \Omega.m$ and $500\ \Omega.m$ associated to the left and right mediums.

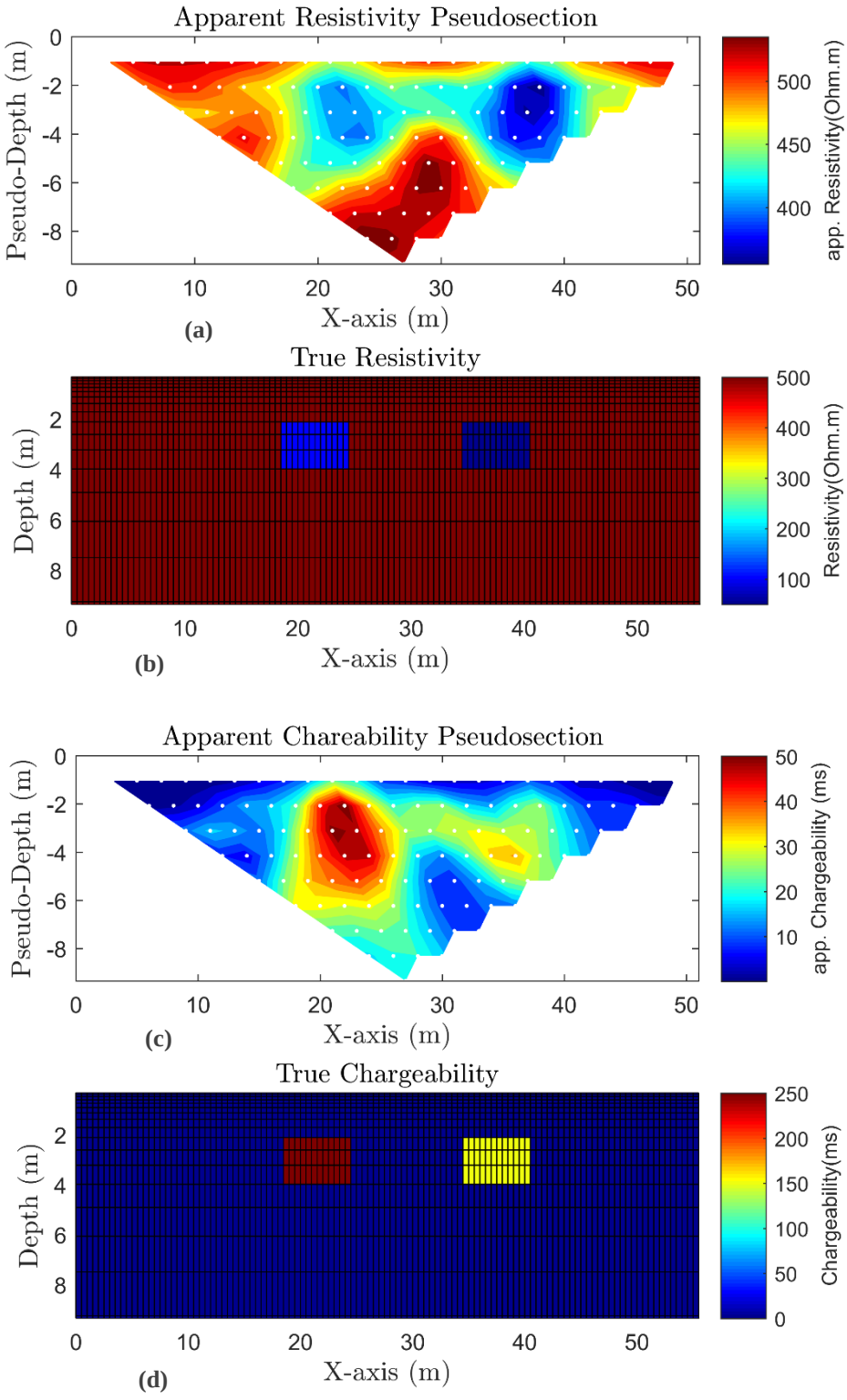

Figure 11. Representation of the apparent, a) resistivity and c) chargeability pseudo-sections derived from the synthetic models of b) resistivity and d) chargeability using the Wenner array over Example 1.

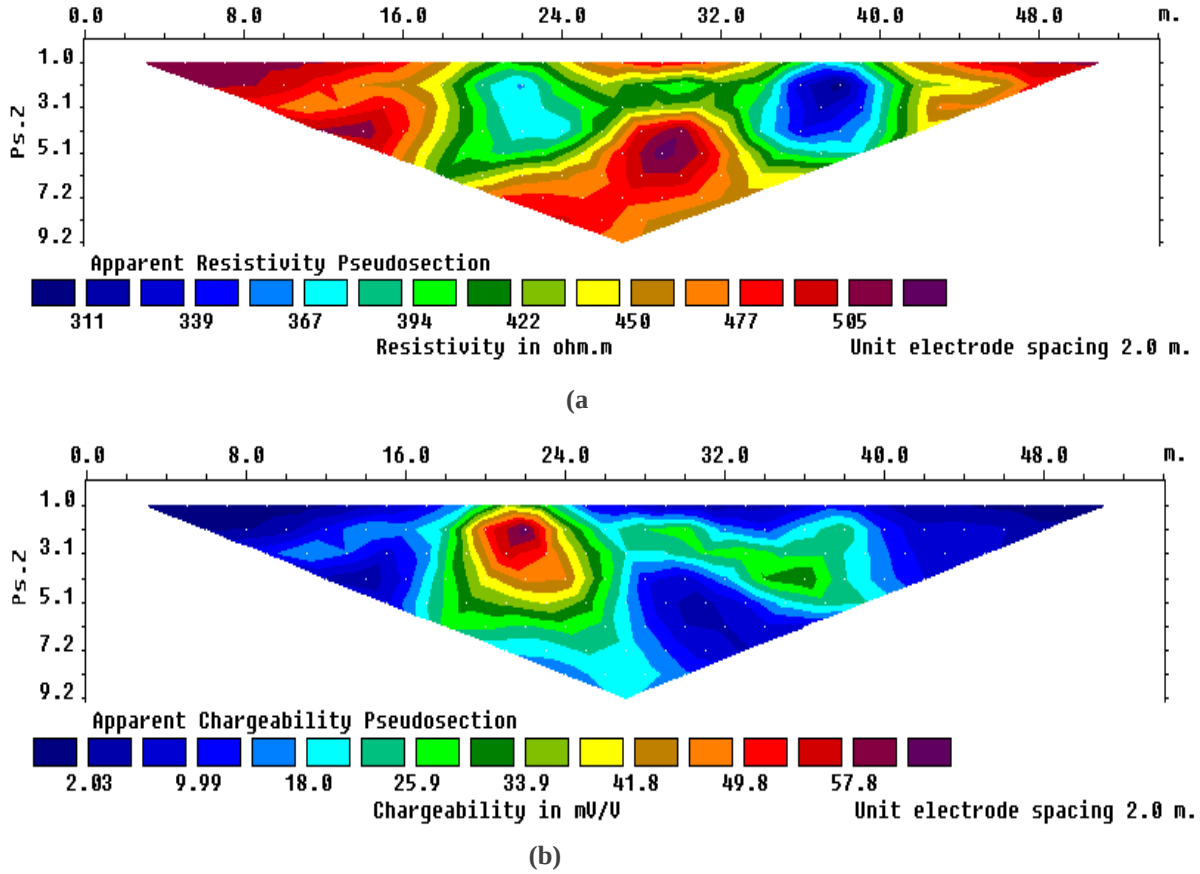

Figure 12. Representation of the apparent, a) resistivity and b) chargeability pseudo-sections derived from RES2DMOD software using the Wenner array over Example 1.

calculated using RES2DMOD software package (Figures 16 and 18). The comparison indicates a close agreement between the resistivity and chargeability pseudo-sections derived by RES2DMOD and those of RESIP2DMODE. In the results represented for both examples, the models are parameterized by equally and logarithmically spaced cells in x and z directions, respectively. In addition, to reduce the effect of the singularity, the vertical discretization is considered very fine grid mesh. However, this strategy in 3D modeling significantly increases the computational expense.

5 Discussion

A reliable resistivity and induced polarization inversion modeling is highly dependent on the accuracy of the forward calculations. So far, several packages of the resistivity and IP forward modeling in the frame of different programming languages have been presented. Despite of the efficiency of the proposed modelling packages, they often include ambiguous and complex scripts which makes it hard to understand and develop them. This motivates and supports the need for open and simple software for the numerical calculation of the 2D electrical potential distribution using the finite difference algorithm. RESIP2DMODE provides a practical graphical user interface designed for functionality and ease of use to visualize the apparent resistivity and induced polarization with respect to the simulated model. The presented package permits the simulation of complicated geometries and conductivity distributions on standard computers. In the previous section,

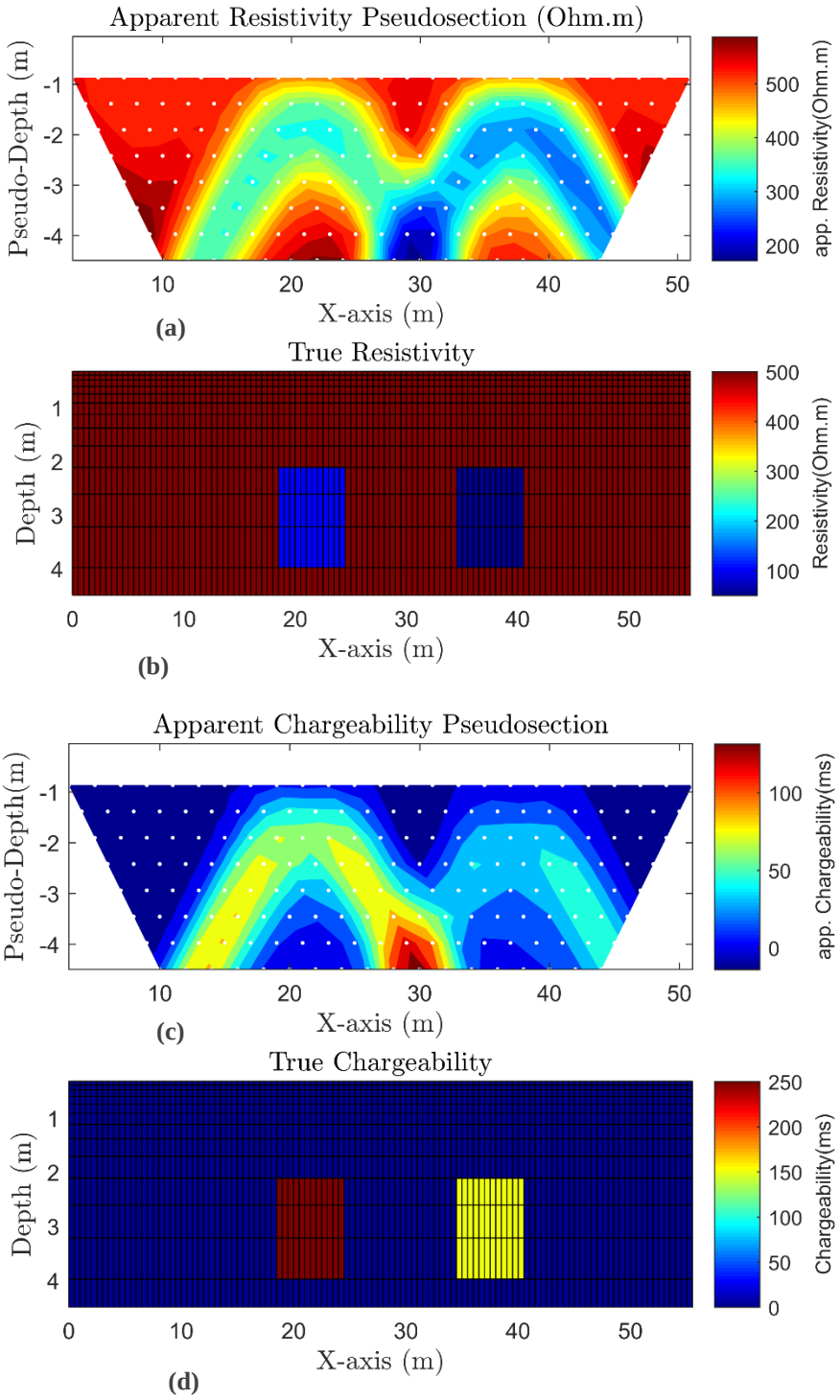

Figure 13. Representation of the apparent, a) resistivity and c) chargeability pseudo-sections derived from the synthetic models of b) resistivity and d) chargeability using the Dipole-Dipole array over Example 1.

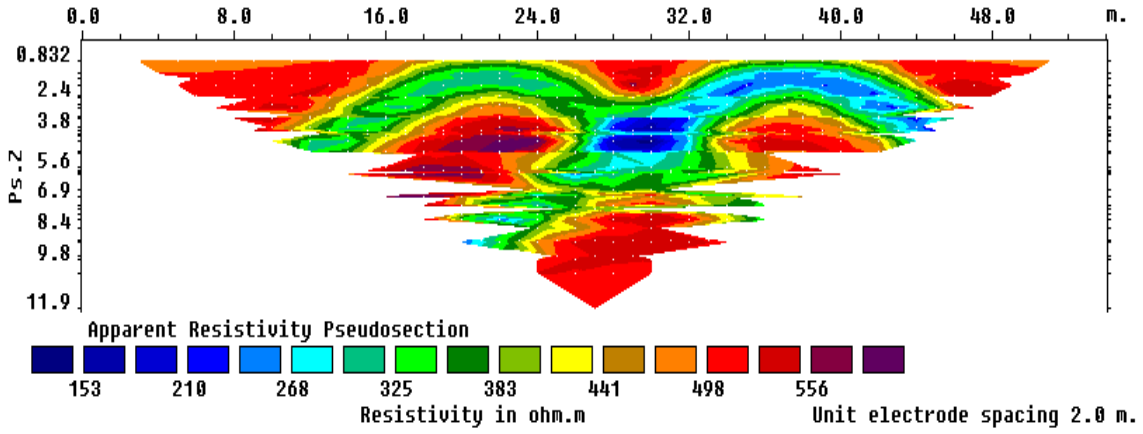

(a)

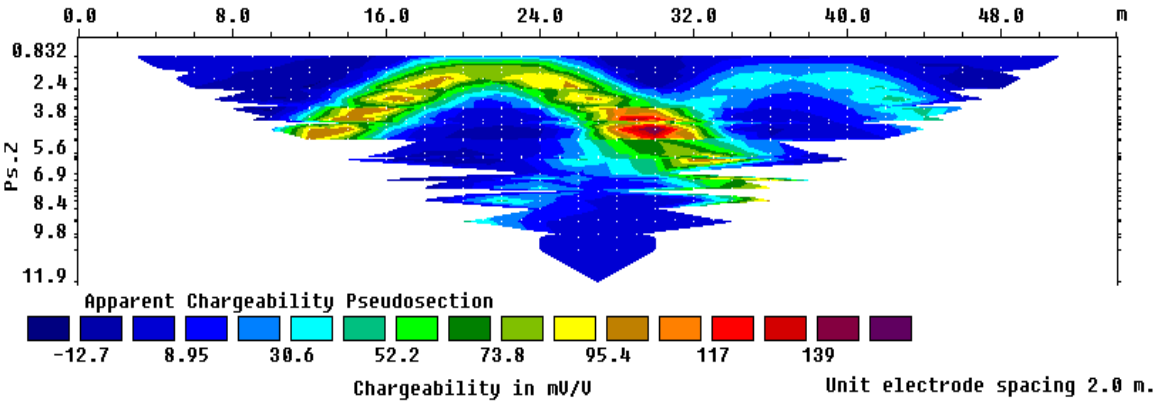

(b)

Figure 14. Representation of the apparent, a) resistivity and b) chargeability pseudo-sections derived from RES2DMOD software using the Dipole-Dipole array over Example 1.

initially, the performance of the proposed software was demonstrated presenting the results of the analytical solution and the numerical algorithm on the horizontal and vertical contacts. In the case of horizontal and vertical contacts, a good agreement was found between the analytical and numerical solutions. However, this small difference between the resistivity values can be relatively removed using source singularity correction, particularly for resistivity values close to the source position. Note that the numerical results are strongly dependent on the mesh size and the extension of the boundaries. A fine mesh significantly increases the accuracy but to the expense of computational cost. For instance, in the vertical model (Fig. 10), there is a strong contrast between the two bodies. As a consequence, a fine mesh is required. This can lead to computer memory issues, especially in the 3D case. Although much effort may be to find a compromise between accuracy and efficiency, the user should adjust the size of the mesh accordingly. Then, for further appraisal, the resulting simulation of two models are compared with a commercial software (RES2DMOD) so that a visually close similarity was demonstrated between the apparent resistivity and induced polarization distribution of the proposed software and RES2DMOD.

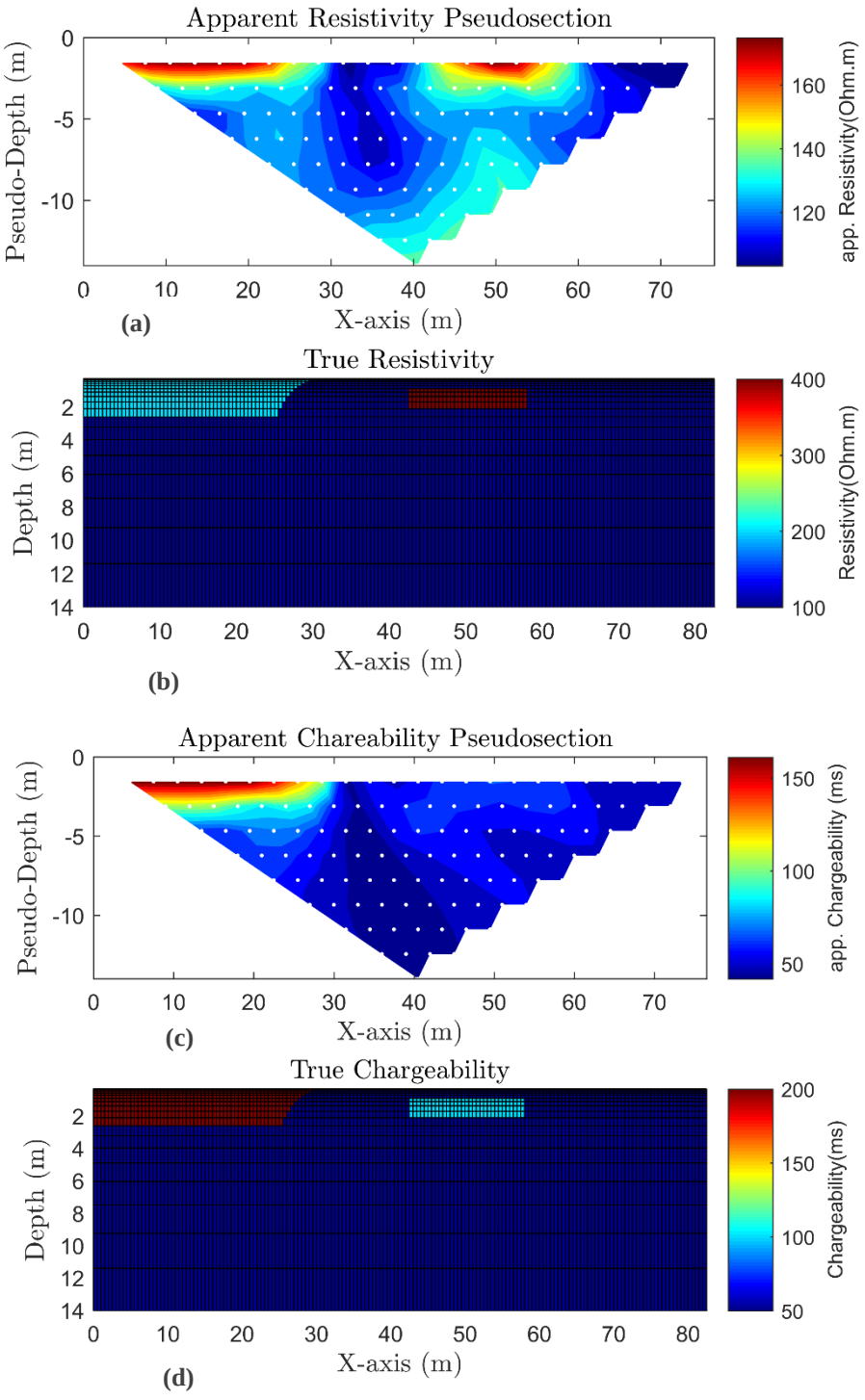

Figure 15. Representation of the apparent, a) resistivity and c) chargeability pseudo-sections derived from the synthetic models of b) resistivity and d) chargeability using the Wenner array over Example 2.

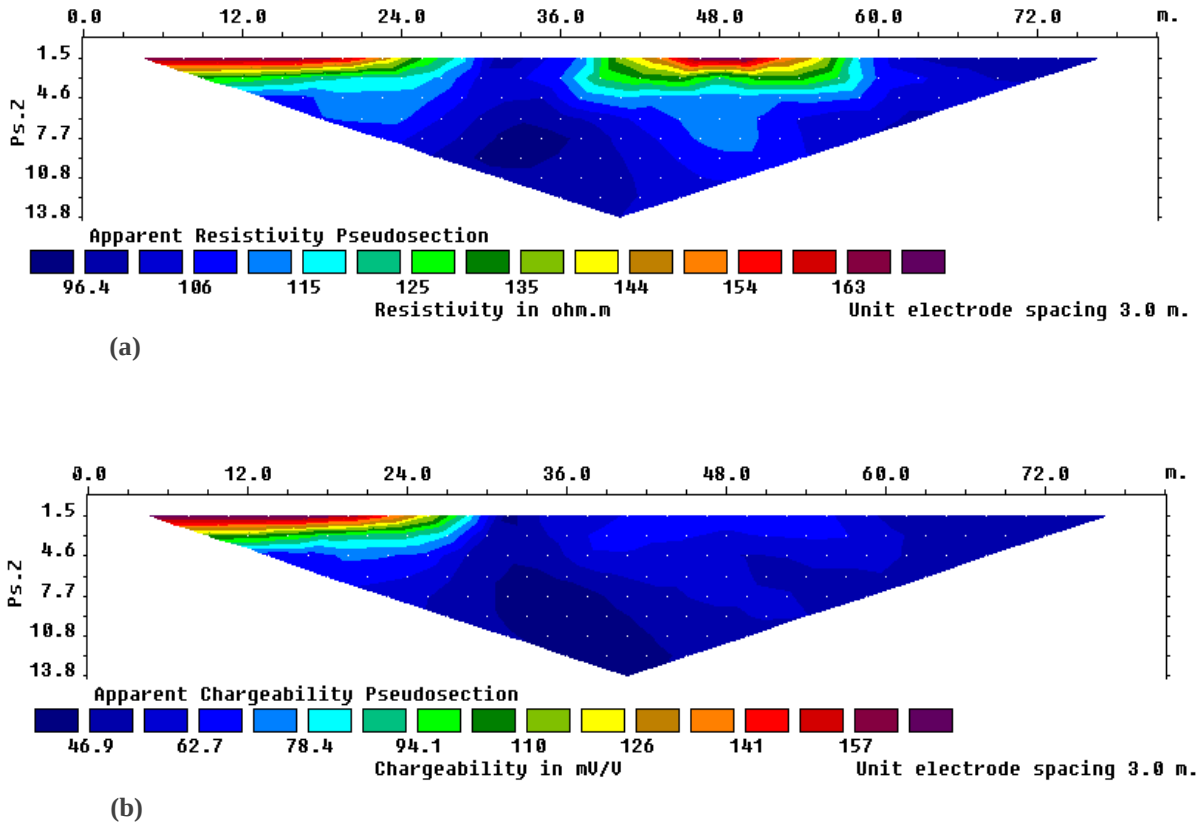

Figure 16. Representation of the apparent, a) resistivity and b) chargeability pseudo-sections derived from RES2DMOD software using the Wenner array over Example 2.

6 Conclusions

Whereas the accuracy of the forward algorithm strongly affects the quality of the inversion result, this paper has focused on developing a MATLAB-based two-dimensional resistivity and induced polarization namely RESIP2DMODE using the finite-difference discretization. The current package can be a user-friendly tool for solving the current flow into the earth's surface through solving the Poisson's equation. Furthermore, the practical user interface of the program can help students and researchers to enhance physical understanding of the geo-electrical responses as well as to recognize the sensitivity of the most commonly used electrode configurations on different situations of the subsurface earth models prior to real field surveys. The accuracy of the package was first tested based on the comparison between the analytical and numerical solutions on horizontal and vertical contacts. The results showed a close agreement between the analytical and numerical responses. In addition, we calculated the resistivity and chargeability responses of a simple model and a complicated model in the frame of the pseudo-sections. RESIP2DMODE is an open-source package that can be extended and upgraded by potential users and developers.

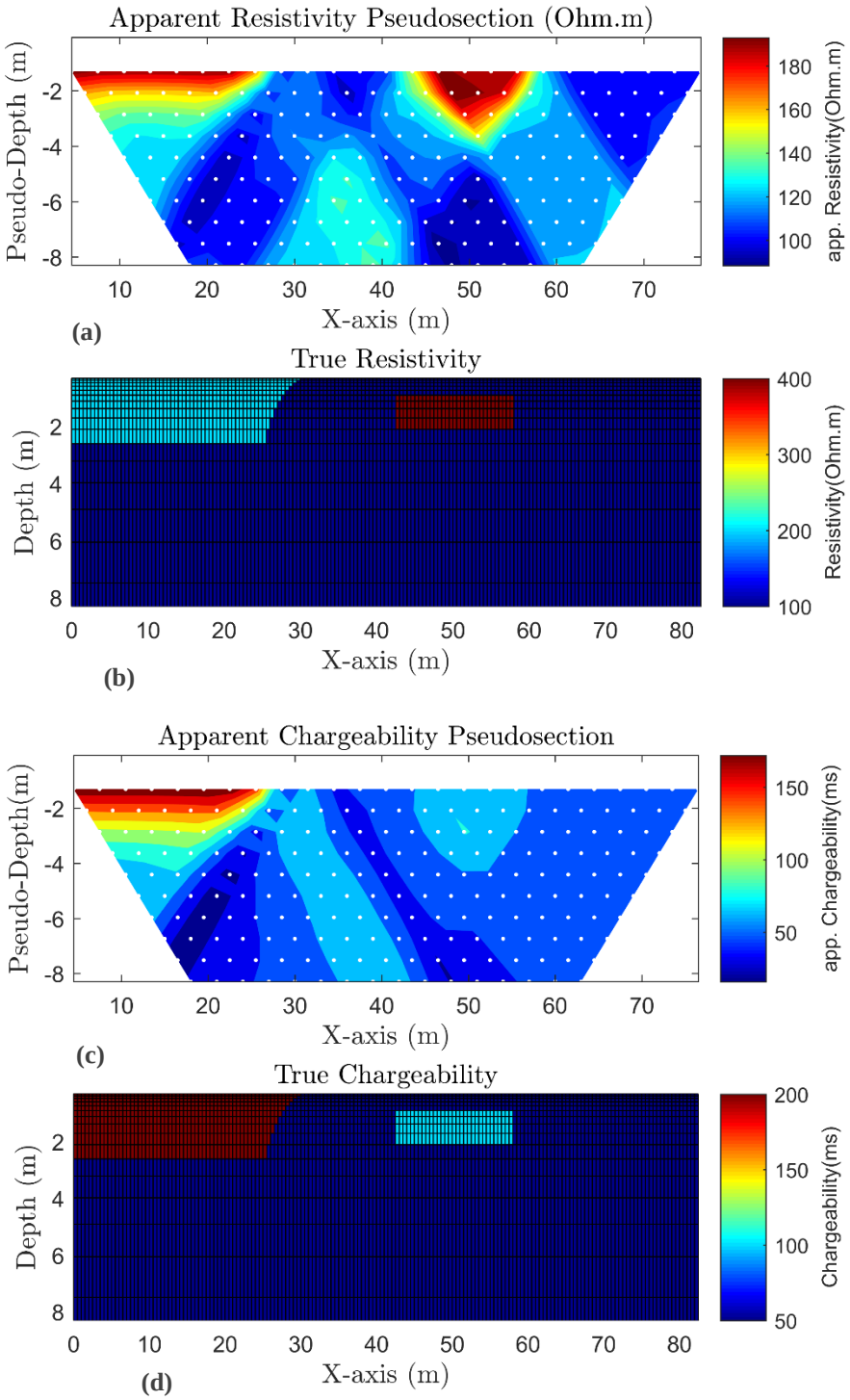

Figure 17. Representation of the apparent, a) resistivity and c) chargeability pseudo-sections derived from the synthetic models of b) resistivity and d) chargeability using the Dipole-Dipole array over Example 2.

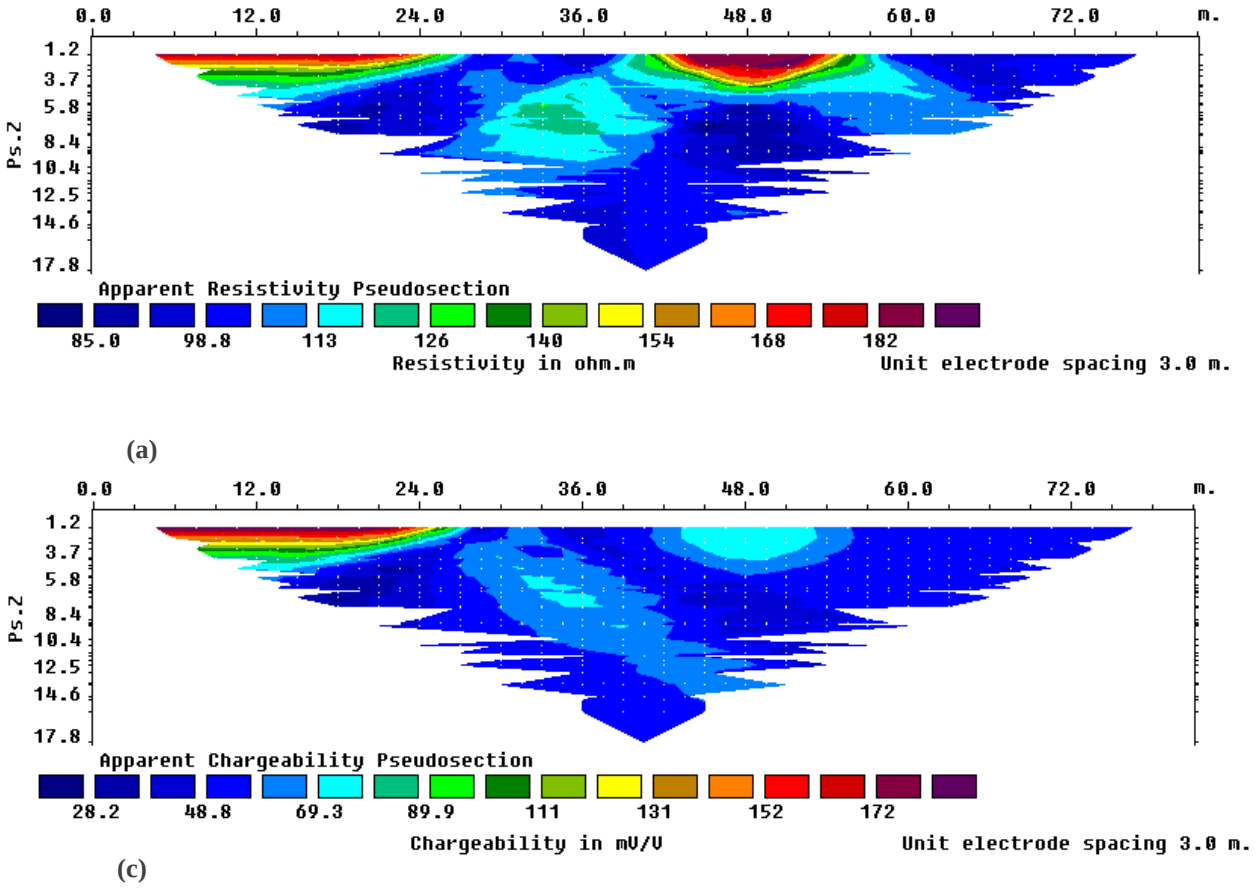

Figure 18. Representation of the apparent, a) resistivity and b) chargeability pseudo-sections derived from RES2DMOD software using the Dipole-Dipole array over Example 2.

Availability of the source code

The program was written on a computer with Intel® Core™ i5- 3337U Processor (1.8 GHz microprocessor) and 8 GB RAM. The source code and supplementary files of the software can be found at http://www.ijgeophysics.ir. There is no specific setup procedure. The program may be run by calling the main function RESIP2DMODE.m from the MATLAB command line.

Acknowledgments

We are grateful to Institute of Geophysics, University of Tehran for all its support. The authors also thank the editor and anonymous reviewers for the constructive and relevant suggestions.

References

Akca, I., 2016, LRIS2D: a MATLAB package for the 2D inversion of DC resistivity/IP data. Acta Geophysica, 64(2), 443–462.

Befus, K. M., 2017, pyres: A Python Wrapper for Electrical Resistivity Modeling with R2, Journal of Geophysics and Engineering, 15, 338–346.

Dahlin, T., Rosqvist, H., Leroux, V., 2010. Resistivity-IP for landfill applications. First Break, 28(8), 101–105.

Demkowicz, L., 2007, Computing with Hp-Adaptive Finite Elements. Chapman and Hall/CRC.

Dey, A. and Morrison, H. F., 1979a, Resistivity modeling for arbitrarily shaped three-dimensional structures. Geophysics, 44(4), 753–780.

Gazoty, A., Fiandaca, G., Pedersen, J., Auken, E., Christiansen, A.V., 2012, Mapping of land-fills using time-domain spectral induced polarization data: the Eskelund case study. Near Surf. Geophys., 10, 575–586.

Günther, T., 2004, Inversion Methods and Resolution Analysis for the 2D/3D Reconstruction of Resistivity Structures from DC Measurements. PhD thesis, Freiberg University of Mining and Technology.

Günther, T., Rücker, C., and Spitzer, K., 2006, 3-d modeling and inversion of DC resistivity data incorporating topography - Part II: Inversion. Geophys. J. Int., 166(2):, 506-517.

Hughes, T. J. R., 1987, The Finite Element Method. Linear Static and Dynamic Finite Element Analysis. Prentice Hall, Englewood Cliffs, NJ.

Loke, M. H, 2014, RES2DMOD ver. 3.01: Rapid 2D resistivity forward modeling using the finite-difference and finite-element methods, Geotomo Software. https://www.geotomosoft.com.

Lowry, T., Allen, M. B., and Shive, P. N., 1989, Singularity removal: A refinement of resistivity modeling techniques. Geophysics, 54(6), 766–774.

McGillivray, P. R., 1992, Forward modeling and inversion of DC resistivity and MMR data. Ph.D. thesis: University of British Columbia.

Mendez-Delgado, S., Gomez-Trevino, E., and Perez-Flores, M. A., 1999, Forward modelling of direct current and low-frequency electromagnetic fields using integral equations: Geophysical Journal International, 137, 336–352.

Pidlisecky, A., Knight, R., 2008, FW2_5D: A MATLAB 2.5-D electrical resistivity modeling code. Computers & Geosciences, 34, 1645–1654.

Qiang, J. K., Han, X., and Dai, S.K., 2013, 3-D DC resistivity inversion with topography based on regularized conjugate gradient method. International Journal of Geophysics, Article ID 931876.

Rücker, C., Günther, T., and Spitzer, K., 2006, Three-dimensional modelling and inversion of dc resistivity data incorporating Topography-I. Modelling. Geophysical Journal International, 166, 495–505.

Rücker, C., Günther, T., Wagner, F.M., 2017, pyGIMLi: an open-source library for modelling and inversion in geophysics. Comput. Geosci., 109, 106–123.

Spitzer, K., and Wurmstich, B., 1995, Speed and accuracy in 3d resistivity modeling. In 3D EM Symposium, Ridgefield, Connecticut.

Telford, W., Geldart, L., Sheriff, R., Keys, D., 1991, Applied Geophysics. Cambridge University Press.

Wu, X. P., 2003, A 3-D finite-element algorithm for DC resistivity modeling using the shifted incomplete Cholesky conjugate gradient method. Geophysical Journal International, 154, 947–956.

Yuan, Y., J. Qiang, J. Tang, Z., Ren, and Xiao, X., 2016, 2.5D direct-current resistivity forward modelling and inversion by finite-element–infinite-element coupled method. Geophysical Prospecting, 64, 767–779.

Zhang, J., Mackie, R. L., and Madden, T. R., 1995, 3-d resistivity forward modeling and inversion using conjugate gradients. Geophysics, 60(5), 1313–1325.